PHYSICAL REVIEW B **80**, 214430 (2009)

# Single-crystal $^{31}$P NMR studies of the frustrated square-lattice compound $Pb_2(VO)(PO_4)_2$

R. Nath,[1,2,*] Y. Furukawa,[1] F. Borsa,[1,3] E. E. Kaul,[2] M. Baenitz,[2] C. Geibel,[2] and D. C. Johnston[1]
[1]*Ames Laboratory and Department of Physics and Astronomy, Iowa State University, Ames, Iowa 50011, USA*
[2]*Max Planck Institut für Chemische Physik Fester Stoffe, Nöthnitzer Str. 40, 01187 Dresden, Germany*
[3]*Dipartimento di Fisica "A. Volta," Università di Pavia, I-27100 Pavia, Italy*
(Received 18 September 2009; revised manuscript received 4 December 2009; published 31 December 2009)

The static and dynamic properties of $V^{4+}$ spins ($S=1/2$) in the frustrated square-lattice compound $Pb_2(VO)(PO_4)_2$ were investigated by means of magnetic susceptibility $\chi$ and $^{31}$P nuclear magnetic resonance (NMR) shift ($K$) and $^{31}$P nuclear spin-lattice relaxation rate $1/T_1$ measurements on a single crystal. This compound exhibits long-range antiferromagnetic order below $T_N \simeq 3.65$ K. NMR spectra above $T_N$ show two distinct lines corresponding to two inequivalent P sites present in the crystal structure. The observed asymmetry in hyperfine coupling constant for the in-plane (P1) P site directly points toward a distortion in the square lattice at the microscopic level, consistent with the monoclinic crystal structure. The nearest- and next-nearest-neighbor exchange couplings were estimated by fitting $K$ versus temperature $T$ by a high-temperature series expansion for the spin susceptibility of the frustrated square lattice to be $J_1/k_B=(-5.4\pm0.5)$ K (ferromagnetic) and $J_2/k_B=(9.3\pm0.6)$ K (antiferromagnetic), respectively. $1/(T_1T\chi)$ is almost $T$ independent at high temperatures due to random fluctuation of spin moments. Below 20 K, the compound shows an enhancement of $1/(T_1T\chi)$ which arises from a growth of antiferromagnetic spin correlations above $T_N$. Below $T_N$ and for the field applied along the $c$ axis, the NMR spectrum for the P1 site splits into two satellites and the spacing between them increases monotonically with decreasing $T$ which is a direct evidence of a columnar antiferromagnetic ordering with spins lying in the $ab$ plane. This type of magnetic ordering is consistent with expectation from the $J_2/J_1 \simeq -1.72$ ratio. The critical exponent $\beta=0.25\pm0.02$ estimated from the temperature dependence of the sublattice magnetization as measured by $^{31}$P NMR at 11.13 MHz is close to the value (0.231) predicted for the two-dimensional XY model.

DOI: 10.1103/PhysRevB.80.214430 PACS number(s): 75.50.Ee, 75.40.Cx, 71.20.Ps

## I. INTRODUCTION

Understanding the ground-state properties of frustrated low-dimensional spin systems is a central issue in current condensed-matter physics. These systems have competing interactions which stabilize different states with distinct symmetries.[1] An interesting phenomenon in spin systems is the formation of a spin liquid with no long-range magnetic order due to suppression by geometric/magnetic frustration. A simple example is the frustrated $S=1/2$ square-lattice (FSL) model. In this model which is also known as $J_1$-$J_2$ model, the spin Hamiltonian is

$$\mathcal{H} = (k_B J_1)\sum_{\langle ij\rangle} \vec{S}_i \cdot \vec{S}_j + (k_B J_2)\sum_{\langle ik\rangle} \vec{S}_i \cdot \vec{S}_k, \qquad (1)$$

where the first sum is over nearest-neighbor (NN) spin pairs and the second is over next-nearest-neighbor (NNN) spin pairs. A positive $J$ corresponds to an antiferromagnetic (AF) exchange interaction and a negative $J$ to a ferromagnetic one. In this paper, $J_1$ and $J_2$ are expressed in temperature units and $k_B$ is Boltzmann's constant. The NN interaction $J_1$ along the side of the square can compete with the NNN interaction $J_2$ along the diagonal of the square if, e.g., both are AF. Recently a generalized phase diagram including both antiferromagnetic and ferromagnetic $J_1$ and $J_2$ has been proposed theoretically based on the frustration ratio $\alpha=J_2/J_1$ or frustration angle $\phi=\tan^{-1}(J_2/J_1)$ as shown in Fig. 1.[2–4] It has three different ordered phases: ferromagnet [FM, wave vector $\mathbf{Q}=(0,0)$], Néel antiferromagnet [NAF, $\mathbf{Q}=(\pi,\pi)$], and columnar antiferromagnet [CAF, $\mathbf{Q}=(\pi,0)$ or $(0,\pi)$]. The critical regions with disordered ground states are predicted to occur at the boundaries NAF-CAF and the CAF-FM which are quantum spin liquid (QSL) phases. A gapless nematic state is suggested for $\alpha\sim-0.5$,[3] while different dimer phases (including resonating-valence-bond-type ones) are claimed to exist for $\alpha$ close to 0.5.[5–8] In addition to its intrinsic interest, a better understanding of the $J_1$-$J_2$ model is expected to play a vital role in understanding the magnetism in recently discovered FeAs-superconducting parent compounds.[9–11]

Experimentally, however, few compounds satisfying the $J_1$-$J_2$ square spin-lattice model have been realized so far. $Li_2VOXO_4$ ($X$=Si,Ge) (Refs. 12 and 13) are two well-studied compounds with antiferromagnetic $J_1$ and $J_2$ and lie in the CAF state of the phase diagram, far away from the QSL regime.[14,15] Recently two new perovskite-type compounds $(CuX)LaNb_2O_7$ ($X$=Cl,Br) were claimed to realize the $J_1$-$J_2$ model with ferromagnetic $J_1$ and antiferromagnetic $J_2$.[16,17] However the validity of the frustrated square-lattice model for these two systems is still unclear.[18] Recent band-structure calculations suggested that despite the layered structure of $(CuCl)LaNb_2O_7$, the spin system has rather pronounced one-dimensional character.[19] The compounds $VOMoO_4$ (Refs. 20 and 21) and $PbVO_3$ (Ref. 22) have been studied in light of the $J_1$-$J_2$ model and were deduced to lie in the NAF region of the phase diagram.

The vanadium phosphates $AA'VO(PO_4)_2$ ($AA'$=$Pb_2$, SrZn, BaZn, and BaCd) present another realization of the $J_1$-$J_2$ model with ferromagnetic $J_1$ and antiferromagnetic $J_2$ and fall in the CAF region of the phase diagram close to the

 

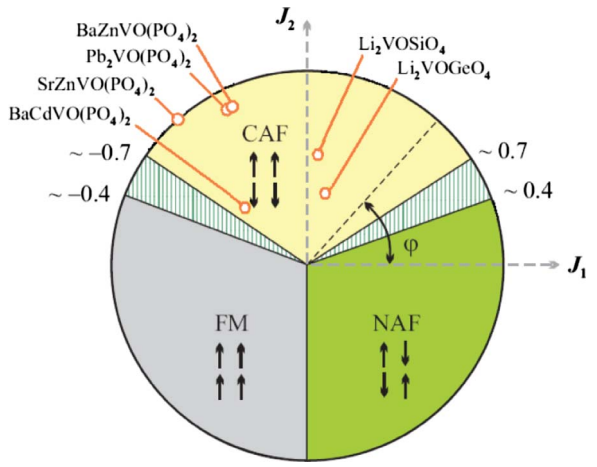


FIG. 1. (Color online) The $J_1$-$J_2$ phase diagram of the two-dimensional spin-1/2 square spin lattice showing different ordered phases and the QSL regimes. The two QSL regimes are the two vertically hatched areas. The boundaries of the QSL regimes are not precisely known. The other regions of the phase diagram contain the FM, CAF, and NAF phases. The location of all the investigated compounds so far in the CAF phase are shown (Refs. 15 and 23–25). The radius of the circle is 12.2 K. Due to relatively large exchange couplings, $PbVO_3$ and $VOMoO_4$ are not included in the phase diagram, for which $J_1=203$ K and $J_2=77$ K (Ref. 22) and $J_1=110$ K and $J_2=22$ K, Ref. 20, respectively. (After Refs. 25 and 28.)

QSL regime.[23–26] The magnetic properties of these compounds have been recently investigated by means of magnetization,[23,26] heat capacity,[24,25] neutron scattering,[27,28] and muon spin resonance[29] ($\mu$SR) experiments. All these measurements were done on polycrystalline materials. However a clear picture about the spin dynamics in these compounds requires measurements on single crystals. Here we present $^{31}$P NMR and magnetic susceptibility $\chi$ measurements on a large single crystal of $Pb_2VO(PO_4)_2$.

$Pb_2(VO)(PO_4)_2$ crystallizes in a monoclinic structure with space group $P2_1/a$ and lattice parameters $a=8.747(4)$ Å, $b=9.016(5)$ Å, $c=9.863(9)$ Å, and $\beta=100.96(4)°$.[30] The structure of $Pb_2(VO)(PO_4)_2$, presented in the upper panel of Fig. 2, is composed of $[VOPO_4]$ layers extending parallel to the *ab* plane which are separated along the *c* axis by Pb atoms and isolated $PO_4$ tetrahedra as shown. The layers are slightly modulated due to lack of tetragonal symmetry. It is important to mention here that there are two inequivalent phosphorus sites (P1 and P2) present in the crystal structure. The $[VOPO_4]$ layers are formed by corner-sharing $V^{4+}O_5$ pyramids with $P1O_4$ tetrahedra while the other site forms isolated $P2O_4$ tetrahedra lying between the $[VOPO_4]$ layers. Thus the P1 site is expected to be strongly coupled and the P2 site weakly coupled to the $V^{4+}$ ($3d^1$, $S=1/2$) spins. In the lower panel of Fig. 2 a section of the *ab* plane is shown. In the approximate $V_4$ square A-B-C-D shown, the $V^{4+}$ spins interact via a V-O-P1-O-V pathway involving two inequivalent oxygen atoms. The distances and angles of the pathways between the different V spins are also different which reflects the inequivalent superexchange paths. We have listed in Table I the distances between the pairs of four $V^{4+}$ spins A, B, C, D, and the angles between them. Small differences are seen in the distances along the edges, the angles between the edges, and the distances along the diagonals from square symmetry, indicating a small distortion of the square.

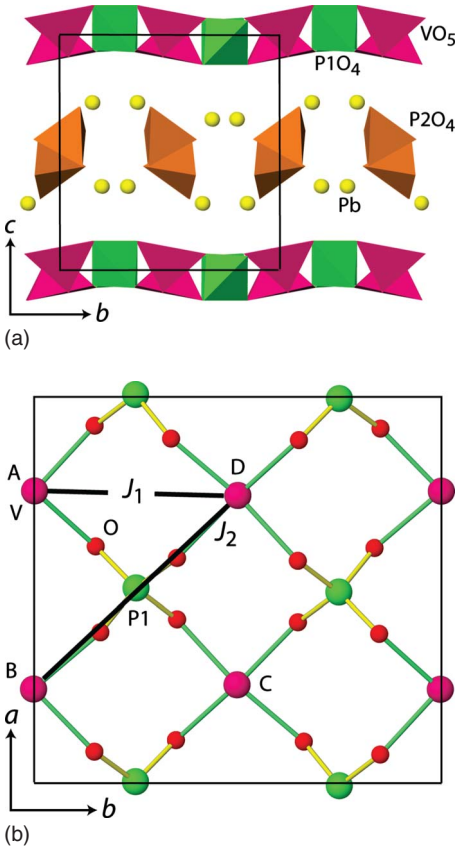


FIG. 2. (Color online) Upper panel: schematic of $[VOPO_4]$ layers in $Pb_2(VO)(PO_4)_2$ running parallel to the *ab* plane. Lower panel: projection onto the *ab* plane of the unit cell showing the arrangement of $VO_5$ pyramids and $P1O_4$ tetrahedra in the plane. The approximate square lattice formed by four $V^{4+}$ spins (labeled as A, B, C, and D) is also shown indicating the nearest-neighbor ($J_1$) and next-nearest-neighbor ($J_2$) exchange interactions.

The exchange interactions $J_1$ and $J_2$ between V spins-1/2 in $Pb_2VO(PO_4)_2$ were reported to be −6.0 and 9.8 K, respectively, and the compound was reported to undergo antiferromagnetic ordering at $T_N \simeq 3.65$ K, likely of CAF type.[23] Recently Tsirlin and Rosner[31] pointed out theoretically from band-structure calculations that due to the reduced symmetry the $J_1$ and $J_2$ values within the $V_4$ square are multivalued:

TABLE I. The distance between pairs of $V^{4+}$ spins along the edges and along the diagonals, and the interior angle between them, for the approximately square lattice shown in the lower panel of Fig. 2 for $Pb_2VO(PO_4)_2$.

| V-V pair | AB | BC | CD | DA | AC | BD |
|---|---|---|---|---|---|---|
| Edges (Å) | 4.669 | 4.665 | 4.669 | 4.410 | | |
| Diagonals (Å) | | | | | 6.267 | 6.295 |
| | ∠ABC | ∠BCD | ∠CDA | ∠DAB | | |
| Angles (deg) | 84.34 | 84.82 | 87.25 | 87.75 | | |

$(J_1',J_1'')$ and $(J_2',J_2'')$, respectively, and the experimental estimates of $J_1$ and $J_2$ should be considered as averaged NN and NNN couplings: $\bar{J}_1=(J_1'+J_1'')/2$ and $\bar{J}_2=(J_2'+J_2'')/2$. From neutron-scattering experiments, a diffuse magnetic background was observed in the paramagnetic state at $T=20$ K which persists well below $T_N$. The ground state was suggested to be CAF type with a reduced ordered moment ($\mu \simeq 0.5\mu_B/V^{4+}$), where $\mu_B$ is the Bohr magneton.[27,28] For a spin-1/2 with g-factor $g=2$, one would expect an ordered moment $\mu=gS\mu_B=1\mu_B$ per V atom. The diffuse background and the reduced ordered moment may be indications of quantum disorder predicted theoretically near the QSL regime.[3] $\mu$SR experiments also show a broad distribution of field at the muon site below $T_N$ suggesting possible structural and/or magnetic disorder.[29] The temperature dependence of the longitudinal muon relaxation rate above $T_N$ and of the order parameter below $T_N$ agree with expectations for the two-dimensional (2D) XY model. Both neutron scattering and $\mu$SR experiments were performed on powder samples. In unpublished work, the $\chi(T)$ of a single crystal above $T_N$ was found to be isotropic along different orientations.[24] Below $T_N$, it is strongly anisotropic with the $b$ axis being the easy axis.[24]

Nuclear magnetic resonance (NMR) is a very powerful experimental tool to extract microscopic information at the individual sites of a crystal. The technique has been applied to many transition-metal oxides and has played a significant role in elucidating their microscopic magnetic characters. In this paper, we report a detailed experimental investigation of static and dynamic properties of $V^{4+}$ spins in $Pb_2(VO)(PO_4)_2$ by means of $^{31}$P NMR and $\chi$ measurements. We have carried out $^{31}$P NMR not only on a polycrystalline sample but also on a large single crystal in order to shed light on the spin structure and possible quantum disorder in $Pb_2(VO)(PO_4)_2$.

## II. EXPERIMENTAL

Syntheses of the polycrystalline sample and of the crystal are reported in Refs. 29 and 30, respectively. The NMR measurements were carried out using pulsed NMR techniques on $^{31}$P (nuclear spin $I=1/2$ and gyromagnetic ratio $\gamma_N/2\pi=17.237$ MHz/T) nuclei in the temperature range $1.5 \leq T \leq 300$ K. Laue x-ray backscattering measurements previously determined in Ref. 24 the orientation of the crystal axes with respect to the crystal faces for the crystal on which NMR measurements were performed. We have done the NMR measurements at two different radio frequencies of 70 and 11.13 MHz which correspond to an applied field of about 4.06 and 0.65 T, respectively. Spectra were obtained either by Fourier transform of the NMR echo signals or by sweeping the field. The NMR shift $K=(\nu-\nu_{ref})/\nu_{ref}$ was determined by measuring the resonance frequency of the sample ($\nu$) with respect to nonmagnetic reference $H_3PO_4$ (resonance frequency $\nu_{ref}$). The $^{31}$P spin-lattice relaxation rate $1/T_1$ was measured by the conventional single saturation pulse method. For the analysis of NMR data, we measured the magnetic susceptibility $\chi(T)$ of the single crystal at 4 T for field applied along $c$ axis in a commercial (Quantum Design) superconducting quantum interference device magnetometer.

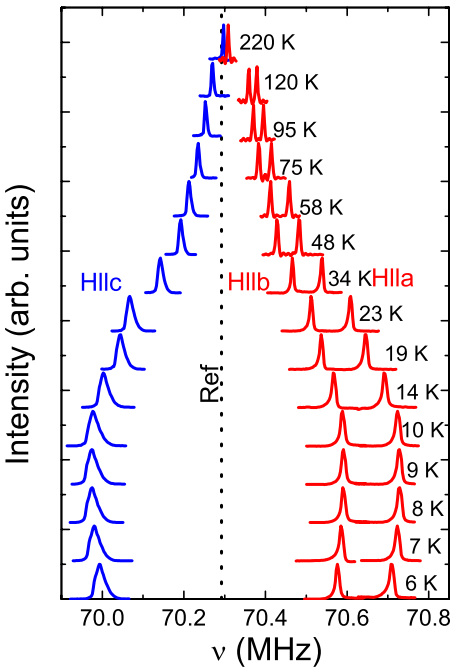


FIG. 3. (Color online) High-field Fourier transform $^{31}$P NMR spectra for the P1 site at different temperatures $T$ ($T>T_N$) and along different orientations for single crystalline $Pb_2(VO)(PO_4)_2$. The vertical dotted line corresponds to the $^{31}$P resonance frequency of the reference sample $H_3PO_4$.

## III. RESULTS

### A. NMR spectra above $T_N$

The $^{31}$P nucleus has nuclear spin $I=1/2$. For a $I=1/2$ nucleus one expects a single spectral line for each inequivalent P site.[32] As shown in the crystal structure (Fig. 2), $Pb_2VO(PO_4)_2$ has two inequivalent P sites. We indeed observed two narrow spectral lines corresponding to the two P sites for all three orientations of the crystal above $T_N$ (e.g., see $^{31}$P NMR spectra at 4.27 K in Fig. 7). For each P site the line position was found to shift with temperature. However for the strongly coupled P1 site the shift was found to be much stronger compared to the weakly coupled P2 site and is also strongly orientation dependent. In the present work we have mainly focused on the P1 site and therefore data for the P2 site are not shown. Figure 3 shows the $^{31}$P NMR spectra for the P1 site measured on a single crystal at different temperatures and field applied along different orientations.

Figure 4(a) presents the temperature dependence of $K$ for the P1 site derived from the data in Fig. 3. It shows a strong anisotropy along different directions. Along the $a$ and $b$ axes it shows a strong positive shift while along the $c$ axis it shows a strong negative shift. On the other hand for the P2 site the shift is very weak. The stronger and weaker shifts for the P1 and P2 sites, respectively, suggest that the former one is strongly coupled while the latter one is weakly coupled to the $V^{4+}$ spins, consistent with expectation from the crystal

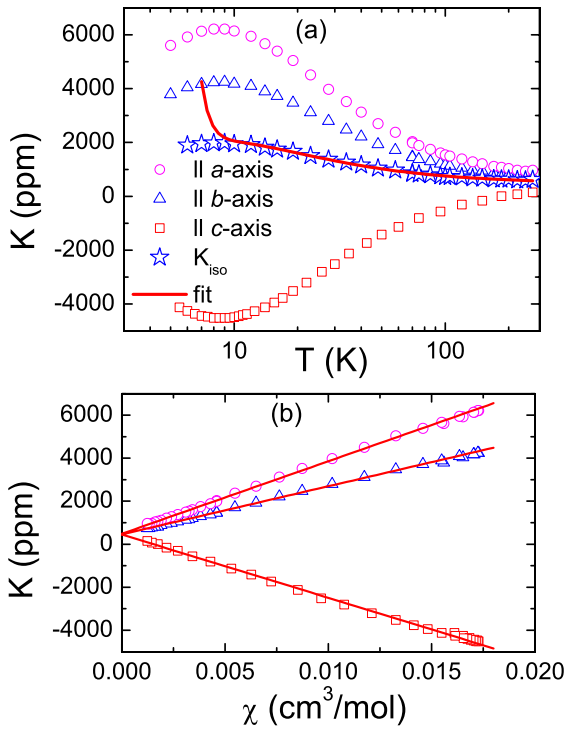


FIG. 4. (Color online) (a) Temperature-dependent NMR shift $K$ vs $T$ for the P1 site along different field orientations. The solid line is the fit of $K_{iso}$ by Eq. (2). (b) $^{31}$P shift $K$ vs $\chi$ measured at 4 T is plotted with temperature as an implicit parameter for all three orientations. The solid lines are linear fits.

structure. The temperature dependence of the isotropic $^{31}$P1 NMR shift $K_{iso}$ was calculated as $K_{iso}=(K_a+K_b+K_c)/3$ and is also shown in Fig. 4(a). It shows a marked $T$ dependence like $\chi(T)$.[24] At high-temperatures $K_{iso}$ varies in a Curie-Weiss manner and then passes through a broad maximum at around 9 K reflecting low-dimensional short-range antiferromagnetic ordering. Since $\chi(T)$ for the single crystal at $T>T_N$ is isotropic along different orientations,[24] this anisotropic $K(T)$ is likely due to asymmetry in the hyperfine coupling constant between the $V^{4+}$ spins and the P nuclear spins.

A $^{31}$P spectrum on a polycrystalline sample is shown in Fig. 5. Along with the most intense central line there is a broad background containing extra shoulderlike features on either side. In an attempt to fit the experimental spectra we assumed that the central part with a small asymmetry comes from the weakly coupled P2 site and the broader one with large asymmetry is from the strongly coupled P1 site. In this way the superposition of these two spectra gives a reliable fit as shown in Fig. 5. One can see in Fig. 5 that for the broad spectrum there are three shoulderlike features clearly visible. These shoulder positions were found to shift with temperature. We took the derivative of the spectra and picked the point of inflection for each shoulder as a function of temperature (not shown) and they overlap nicely with the single crystal $K(T)$ confirming that the shoulders are due to anisotropic shift at the P1 site. On the other hand the narrow line (P2 site) was found to shift very weakly with temperature.

The NMR shift is a direct measure of the spin susceptibility $\chi_{spin}$, and quite generally $K(T)$ is written in terms of $\chi_{spin}(T)$ as[33]

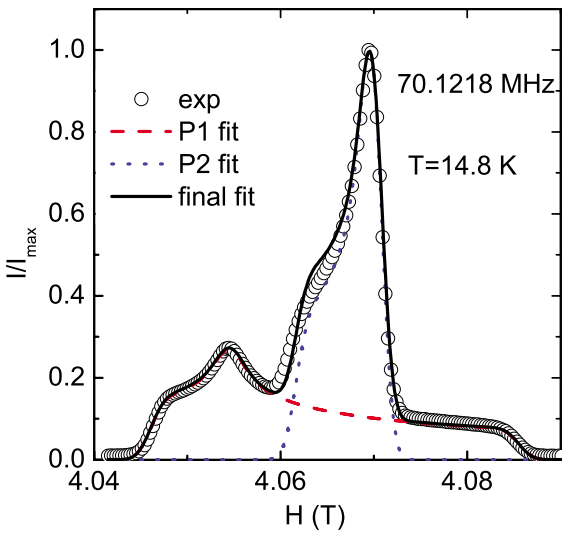


FIG. 5. (Color online) The $^{31}$P NMR spectrum at 14.8 K measured at 70.1218 MHz on a polycrystalline $Pb_2(VO)(PO_4)_2$ sample (open circles). The dashed and dotted lines are the theoretical fits for the P1 and P2 sites, respectively, and the solid line is the total fit which is a superposition of the P1 and P2 fits. The NMR shift values along the $a$, $b$, and $c$ directions obtained from the fitting are $K_a \simeq 5500$ ppm, $K_b \simeq 3430$ ppm, and $K_c \simeq -4160$ ppm and $K_a \simeq 1960$ ppm, $K_b \simeq -342$ ppm, and $K_c \simeq -512$ ppm for the P1 and P2 sites, respectively.

$$K(T) = K_0 + \frac{A_{hf}}{N_A}\chi_{spin}(T), \tag{2}$$

where $K_0$ is the temperature-independent chemical (orbital) shift, $N_A$ is the Avogadro number, $A_{hf}$ is the hyperfine coupling constant between the P nuclear spins and the $V^{4+}$ electronic spins and $\chi_{spin}/N_A$ is expressed in units of $\mu_B$/Oe per electronic spin, which in our case means per formula unit. The conventional scheme for calculating $A_{hf}$ is to take the slope of the $K$ vs $\chi_{spin}$ plot with $T$ as an implicit parameter. Here we mainly focus on the P1 site. For each orientation the $K$ vs $\chi$ plot is fitted very well by a straight line [Fig. 4(b)] over the whole temperature range ($T>T_N$) yielding $A_{hf}=(1882\pm40)$, $(1251\pm42)$, and $-(1642\pm55)$ Oe/$\mu_B$ along the $a$, $b$, and $c$ directions, respectively. The isotropic hyperfine coupling constant is then calculated to be $A_{iso}=(A_a+A_b+A_c)/3=(497\pm46)$ Oe/$\mu_B$.

In order to estimate the exchange couplings $J_1$ and $J_2$, we fitted the temperature dependence of $K_{iso}$ above 15 K by Eq. (2), where $\chi_{spin}$ is the high-temperature series-expansion prediction for the molar spin susceptibility of the frustrated square-lattice model given by[15]

$$\chi_{spin}(T) = \frac{N_A g^2 \mu_B^2}{k_B T}\sum_n \left(\frac{J_1}{k_B T}\right)^n \sum_m c_{m,n}\left(\frac{J_2}{J_1}\right)^m, \tag{3}$$

where $c_{m,n}$ are the coefficients listed in Table I of Ref. 15, $g$ is the $g$-factor, and $k_B$ is the Boltzmann constant. From the electron paramagnetic resonance measurements at room temperature, $g$ parallel ($g_\parallel$) and perpendicular ($g_\perp$) to the $c$ axis were found to be 1.929 and 1.966, respectively.[34] The isotro-

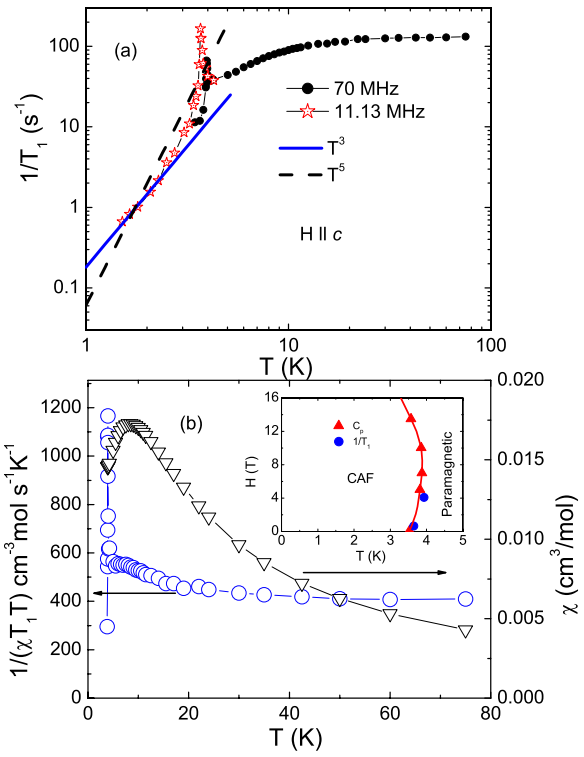


FIG. 6. (Color online) (a) Nuclear spin-lattice relaxation rate $1/T_1$ vs temperature $T$ measured for the P1 site at 70 and 11.13 MHz with the magnetic field applied along the $c$ axis. Below $T_N$ measurements were done at the central field corresponding to the right-hand-side satellite [see Fig. 7(b)]. The solid and dashed lines represent $T^3$ and $T^5$ behaviors, respectively. (b) $1/(\chi T_1 T)$ (left $y$ axis) and $\chi$ (right $y$ axis) plotted as a function of $T$. The inset shows the $H$ vs $T$ phase diagram where $T_N$ values obtained from our $1/T_1$ measurements at the P1 site and the values from heat-capacity $C_p$ measurements (Ref. 24) are plotted.

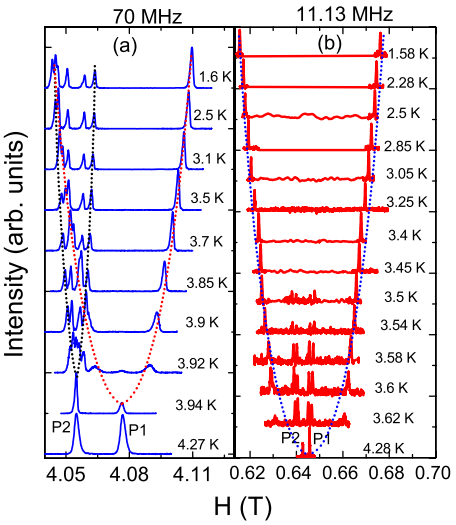


FIG. 7. (Color online) Temperature-dependent $^{31}$P NMR spectra measured at (a) 70.00 MHz and (b) 11.13 MHz for $H \| c$. The spectra in the paramagnetic state split below $T_N$ into two and four lines for the P1 and P2 sites, respectively, due to the internal field $H_{int}$. The dashed lines are guides to the eyes for the shifts of the satellite lines.

pic $g=\sqrt{(g_\parallel^2+2g_\perp^2)/3}$ was calculated to be 1.95 which was kept fixed during the fitting procedure. In this way we obtained $K_0=(462\pm11)$ ppm, $A_{hf}=(481\pm20)$ Oe/$\mu_B$, $J_1=(-5.4\pm0.5)$ K, and $J_2=(9.3\pm0.6)$ K. The fit is shown in Fig. 4(a) as a solid line. These values of $J_1$ and $J_2$ are close to the previously reported values estimated from $\chi(T)$ analysis[23,24] and also consistent with the saturation field obtained from high-field magnetization isotherm measurements.[26] The estimated $A_{hf}$ matches with the $A_{iso}$ calculated above from the $K$-$\chi$ analysis within the error bars.

### B. Nuclear spin-lattice relaxation rate $1/T_1$

The $^{31}$P nuclear spin-lattice relaxation rate $1/T_1$ was measured with the magnetic field applied parallel to the $c$ axis. For a $I=1/2$ nucleus the recovery of the longitudinal magnetization is expected to follow a single-exponential behavior. In $Pb_2VO(PO_4)_2$, the recovery of the nuclear magnetization after a saturation pulse was indeed fitted well by the exponential function

$$1-\frac{M(t)}{M_0}=Ae^{-t/T_1}, \tag{4}$$

where $M(t)$ is the nuclear magnetization at a time $t$ after the saturation pulse and $M_0$ is the equilibrium nuclear magnetization. The temperature dependence of $1/T_1$ measured for the P1 site for $H \| c$ is presented in Fig. 6(a). At high temperatures ($T \gtrsim 20$ K), $1/T_1$ is temperature independent. In the high-temperature limit $T \gg J$, a temperature-independent $1/T_1$ behavior is typical when paramagnetic moments fluctuate fast and at random.[35] With decrease in temperature, $1/T_1$ decreases slowly for $T<15$ K and then shows a peak around 3.93 K. This decrease is very similar to that observed previously in the cases of the antiferromagnetic square lattices $VOMoO_4$ from $^{95}$Mo NMR (Ref. 20) and $[Cu(HCO_2)_2.4D_2O]$ from $^1$H NMR where the decrease in $1/T_1$ above $T_N$ is explained by cancellation of the antiferromagnetic spin fluctuations at the positions of the probed nuclei.[36] Below the peak $1/T_1$ again decreases smoothly toward zero.

For the polycrystalline sample, $1/T_1$ measurements were not possible due to broad spectra and overlapping of signals from the two P sites.

### C. NMR spectra below $T_N$

Below $T_N$ both the P1 and P2 lines were found to split (Fig. 7) indicating that both P sites are experiencing the static internal field in the ordered state. The P1 site line splits into two satellite lines while the P2 site line splits into four satellite lines as a result of the hyperfine field between the P nuclei and the ordered $V^{4+}$ moments. For the 70 MHz measurements [Fig. 7(a)], the left-hand-side satellite of the P1 site overlaps with the four split satellites of the P2 site making it difficult to distinguish the peaks. It is possible to separately measure the spectra for the two different sites by measuring at low frequency and using a faster repetition rate since the relaxation rates associated with the two sites are different (for the P1 site $T_1$ is shorter than for the P2 site). Therefore we remeasured the spectra for the P1 site at 11.13

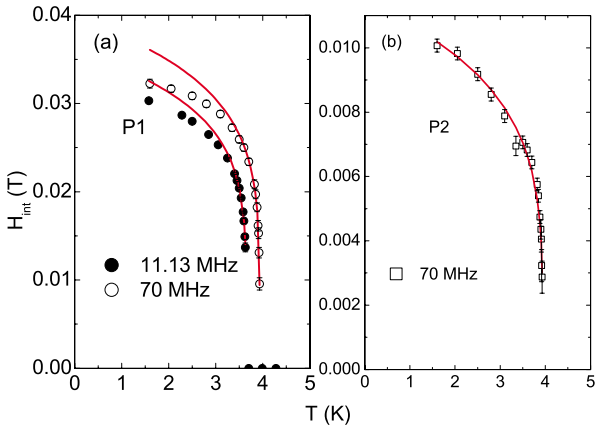


FIG. 8. (Color online) Temperature $T$ dependence of the internal field $H_{\rm int}$ obtained from NMR spectra for $H\|c$ in the ordered state (a) for the P1 site measured at 11.13 and 70 MHz and (b) for the P2 site measured at 70 MHz. $H_{\rm int}$ is proportional to the $V^{4+}$ sublattice magnetization. The solid lines are fits by Eq. (5) to the data, as described in the text.

MHz using a faster repetition rate and the results are presented in Fig. 7(b).

The internal field $H_{\rm int}$, which is proportional to the $V^{4+}$ sublattice magnetization, was determined from half the separation between the split lines. The temperature dependences of $H_{\rm int}$ are shown in Fig. 8 for both the P sites measured for $H\|c$. For the P1 site at 70 MHz, the left-hand-side satellite was chosen as the peak of equal intensity to the right-hand-side satellite. The $H_{\rm int}(T)$ for the P1 site was found to be almost independent of field below $T_{\rm N}$. In order to extract the critical exponent of the order parameter (sublattice magnetization), $H_{\rm int}(T)$ was fitted by the power law

$$H_{\rm int}(T) = H_0\left(1 - \frac{T}{T_{\rm N}}\right)^{\beta}. \tag{5}$$

One can notice that $H_{\rm int}$ decreases sharply on approaching $T_{\rm N}$. For an accurate determination of the critical exponent $\beta$, one needs data points close to $T_{\rm N}$ (i.e., in the critical region). We have estimated $\beta$ by fitting the data points in temperature steps of 0.01 K as close as possible to $T_{\rm N}$ as shown in Fig. 8. For the P1 site at 11.13 MHz, the maximum value of $\beta=0.25\pm0.02$ with $T_{\rm N}\simeq3.655$ K was obtained by fitting the data points (3.58–3.63 K) close to $T_{\rm N}$. By increasing the number of fitting points toward low $T$'s, the $\beta$ value was found to decrease and the minimum value of $\beta=0.15\pm0.02$ with $T_{\rm N}\simeq3.64$ K was obtained by fitting the whole temperature range (1.58–3.63 K). Similarly for the P1 site at 70 MHz, the maximum value of $\beta=0.23\pm0.03$ with $T_{\rm N}\simeq3.933$ K was obtained by fitting data points (3.9–3.93 K) close to $T_{\rm N}$ and it decreases when low-$T$ data points were included. At low $T$'s, $H_{\rm int}$ develops the tendency of saturation and it saturates much faster than expected from mean-field theory [see the deviation of fits in Fig. 8(a) at low $T$s]. On the other hand for the P2 site at 70 MHz, close to $T_{\rm N}$, due to overlapping of the lines from the two P sites an accurate determination of $H_{\rm int}$ was not possible; therefore the data points shown in Fig. 8(b) for the P2 site have large error bars.

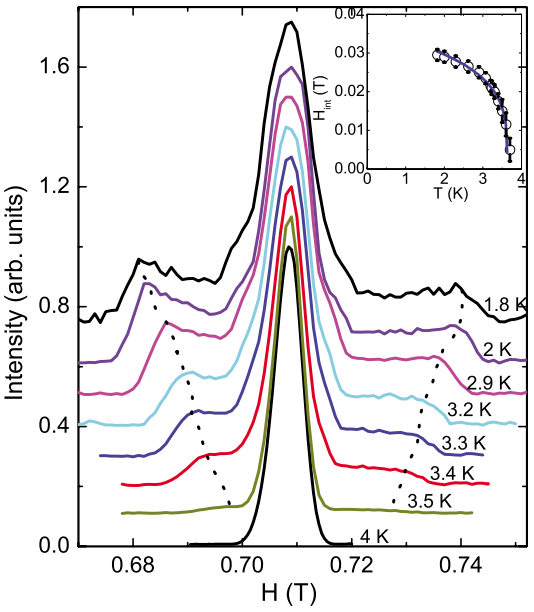


FIG. 9. (Color online) Temperature-dependent $^{31}$P NMR spectra measured at 12 MHz on a polycrystalline sample below $T_{\rm N}$. The dotted lines indicate the splitting of the P1 line. Inset: internal field $H_{\rm int}$ as a function of temperature $T$. The solid line is a fit by Eq. (5).

For the polycrystalline sample below $T_{\rm N}$, the NMR line at 70 MHz was found to broaden abruptly. In order to check whether any extra features could be resolved, we remeasured the spectra at a low frequency (12 MHz) and again with a fast repetition rate. It was found that above $T_{\rm N}$ the line remains narrow and immediately below $T_{\rm N}$ it starts broadening (see Fig. 9). The broad line arising from the P1 site develops two satellites on either side of the central peak that are due to the P2 site. With a decrease in temperature these two satellites move away from each other.[37] We then plotted half the distance between the two satellite positions ($H_{\rm int}$) as a function of temperature (inset of Fig. 9). Fitting the data from 1.7 to 3.6 K by Eq. (5) yielded $\beta=0.25\pm0.07$.

## IV. DISCUSSION

### A. Statics

The exchange couplings extracted from our NMR isoshift data are consistent with the values reported from $\chi(T)$ analysis.[23,24] Based on the $J_2/J_1$ ratio, $Pb_2VO(PO_4)_2$ with $\alpha\simeq-1.72$ is located in the CAF regime of the phase diagram in Fig. 1. In the crystal structure, squares are formed via a V-O-P1-O-V superexchange interaction path. Since P1 is strongly coupled to the $V^{4+}$ spins via hyperfine interaction, any change in the structure properties would be reflected in the $^{31}$P NMR. The total hyperfine coupling constant at the P1 site is generally the sum of transferred hyperfine ($A_{\rm trans}$) and dipolar ($A_{\rm dip}$) couplings produced by $V^{4+}$ spins, i.e., $A_{\rm hf}=z'A_{\rm trans}+A_{\rm dip}$, where $z'$ is the number of nearest-neighbor $V^{4+}$ spins of the P1 site. The anisotropic dipolar couplings were calculated for three orientations of the crystal

using lattice sums with an assumption of $1\mu_B$ magnetic moment on each $V^{4+}$ ion, which are $A^a_{dip}=150$ Oe/$\mu_B$, $A^b_{dip}=170$ Oe/$\mu_B$, and $A^c_{dip}=-320$ Oe/$\mu_B$ along the $a$, $b$, and $c$ directions, respectively. Thus by subtracting the dipolar coupling from the total hyperfine coupling, the transferred hyperfine coupling was obtained to be $A_{trans}=1730$, 1080, and $-1320$ Oe/$\mu_B$, respectively, suggesting that the dominant contribution to the total hyperfine coupling is due to the transferred hyperfine coupling at the P1 site. The transferred hyperfine coupling at the P1 site arises mainly from interactions with the four nearest-neighbor V spins in the plane. The isotropic and anisotropic transferred hyperfine couplings originate from P($3s$)-O($2p$)-V($3d$) and P($3p$)-O($2p$)-V($3d$) covalent bonds, respectively. Since P1 is surrounded by four V ions forming an approximate square lattice in the plane, the experimentally observed asymmetry in total hyperfine field in the plane indicates inequivalent P($3p$)-O($2p$)-V($3d$) bonds for the four nearest-neighbor V ions and hence a distortion in the square lattice, consistent with the low symmetry of the crystal structure as pointed out in Sec. I. Our observations seem to be consistent with the recent theoretical calculation by Tsirlin and Rosner[31] where they have estimated the AFM NNN exchange couplings $J_2'$ and $J_2''$. The ratio is $J_2''/J_2'=0.67$, smaller than the value of unity expected for a regular frustrated square lattice, consistent with a distortion in the square. Theoretical studies have indicated that the frustrating next-nearest-neighbor coupling $J_2$ can lead to a lattice distortion due to spin-lattice coupling.[38,39]

Now we discuss the spin structure in the magnetically ordered state. As shown in Fig. 7, for $H\|c$, the P1 line splits into two lines rather than being simply shifted to lower field in the antiferromagnetically ordered state. We also carried out spectral measurements below $T_N$ for the field applied along $a$ and $b$ axes at 11.6 MHz. For both directions, the NMR line was also found to split but the splitting is much weaker compared to that with the field along the $c$ axis. For instance, at $T\approx 2.9$ K, the internal field $H_{int}$ along the $a$ and $b$ axes are $\sim 5$ and $\sim 10$ Oe, respectively, while along the $c$ axis it is about 250 Oe.[40] Thus the direction of the internal field $H_{int}$ at the P1 site is almost parallel (or antiparallel) to the applied field $H$ along the $c$ axis. In this case the effective field at the P1 site would be $H_{eff}=H\pm H_{int}$. The satellite lines are rather sharp with no striking broadening. Thus the splitting of the NMR line with no broadening is direct evidence of a commensurate magnetic structure. If the magnetic structure were incommensurate with the lattice, the internal field would be distributed and the spectrum would not exhibit sharp resonance lines as seen in Fig. 7. As pointed out before by neutron-scattering experiments, a diffuse magnetic background reminiscent of quantum disorder was observed while approaching $T_N$.[27] In NMR this magnetic background would have appeared as line broadening. Thus our experimentally observed narrow satellites with no further splitting do not indicate the presence of magnetic/structural disorder, which is inconsistent with the interpretations of $\mu$SR (Ref. 29) and neutron-scattering (Ref. 27) results measured on powder samples. At present the origin of this discrepancy is not clear to us. Further inelastic neutron-scattering and $\mu$SR experiments on single crystals are required for a better understanding of this issue.

Our observations are very similar to $^{75}$As NMR measurements on (Ba,Sr,Ca)$Fe_2As_2$ in the stripe-/columnar-type magnetically ordered state.[41–43] According to Kitagawa *et al.*,[41] based on the crystal symmetry of (Ba,Sr,Ca)$Fe_2As_2$ with orthorhombic structure (*Fmmm*), the internal field at the $^{75}$As site is explained by an off-diagonal transferred hyperfine field induced by four nearest-neighbor Fe moments whose direction is in the *ab* plane. In the case of Néel-type AFM order, the $c$ component of $H_{int}$ at the As site is zero due to a perfect cancellation of the off-diagonal hyperfine fields produced by the four Fe moments when the spin moments are in the *ab* plane. Only the stripe-type AFM order can produce a $c$ component of $H_{int}$ at the As site. In the case of $Pb_2VO(PO_4)_2$, the crystal structure is monoclinic ($P2_1/a$) with a lower symmetry. Thus the relationship between $H_{int}$ and the magnetic structure is not trivial. In addition, the hyperfine field at the P1 site contains both transferred and dipolar components. However, it may be possible to consider the present case based on the discussion for (Ba,Sr,Ca)$Fe_2As_2$ systems as a first approximation because the local symmetry in the plane is close to fourfold axial symmetry corresponding to a square lattice formed by V ions with respect to the P1 site. Since the magnetic easy axis is the $b$ axis and the direction of $H_{int}$ is along the $c$ axis in the magnetic ordered state, it is concluded that magnetic order in $Pb_2VO(PO_4)_2$ has a columnar structure with spins in the *ab* plane. Our interpretation in terms of a columnar magnetic structure is consistent with the neutron-scattering experiments.[28] Of course, as we pointed out, the fourfold symmetry of the square lattice is slightly broken due to the lower symmetry of the crystal structure which makes the analysis more complicated. The small $a$ and $b$ components of $H_{int}$ might originate from the nonperfect cancellation of the hyperfine field due to the low-symmetry crystal structure. The observed splitting to four lines of the P2 site spectrum could also be related to such a complication.

### B. Dynamics

The overall temperature-dependent behaviors of $1/T_1$ for both P sites are alike. As shown in Fig. 6(b), $1/(\chi T_1 T)$ above $\sim 20$ K is $T$ independent and increases slowly below 20 K where the system begins to show strong antiferromagnetic short-range correlations. In the same figure $\chi(T)$ is also plotted to highlight the broad maximum corresponding to the short-range correlations. In general, $1/(T_1T)$ is expressed in terms of the dynamic susceptibility $\chi_M(\vec{q},\omega_0)$ per mole of electronic spins as[44–46]

$$\frac{1}{T_1T}=\frac{2\gamma_N^2 k_B}{N_A^2}\sum_{\vec{q}}|A(\vec{q})|^2\frac{\chi_M''(\vec{q},\omega_0)}{\omega_0}, \tag{6}$$

where the sum is over wave vectors $\vec{q}$ within the first Brillouin zone, $A(\vec{q})$ is the form factor of the hyperfine interactions as a function of $\vec{q}$ in units of Oe/$\mu_B$, and $\chi_M''(\vec{q},\omega_0)$ is the imaginary part of the dynamic susceptibility at the nuclear Larmor frequency $\omega_0$ in units of $\mu_B$/Oe. The uniform static molar susceptibility $\chi=\chi_M'(0,0)$ corresponds to the real component $\chi_M'(\vec{q},\omega_0)$ with $q=0$ and $\omega_0=0$. Thus the temperature-independent behavior of $1/(\chi T_1 T)$ above 20 K

in Fig. 6(b) demonstrates that the $T$ dependence of $\Sigma_{\vec{q}}|A(\vec{q})|^2\chi''_M(\vec{q},\omega_0)$ scales to that of $\chi$. On the other hand, a slight increase in $1/(\chi T_1 T)$ below 20 K indicates that $\Sigma_{\vec{q}}|A(\vec{q})|^2\chi''_M(\vec{q},\omega_0)$ increases more than $\chi$ due to the growth of antiferromagnetic correlations with decreasing $T$. There could be two possible sources for this growth of antiferromagnetic correlations. One is Néel-type antiferromagnetic spin fluctuations characterized by the wave vector $\vec{q}=(\pm\pi/a,\pm\pi/b)$ and the other is columnar-type AFM spin fluctuations with $\vec{q}=(\pm\pi,0)$ above $T_N$. The hyperfine form factor at the P1 site can be written as $|A(\vec{q})|^2=\{2A[\cos(q_x a/2)+\cos(q_y b/2)]\}^2$, if P1 is located at the center of the perfect square lattice formed by V ions. In such a case, Néel-type antiferromagnetic spin fluctuations do not contribute to $1/(\chi T_1 T)$ since $|A(\vec{q})|^2$ is zero. However, in $Pb_2VO(PO_4)_2$, since P1 is not located exactly at the center of a square lattice, $A(\vec{q})$ should have a nonzero value. Therefore the enhancement of $1/(\chi T_1 T)$ could be due to the growth of Néel-type AF spin fluctuations which are not completely filtered out at the P1 site. Alternatively, since the AFM ordered state is columnar type as discussed before, if it has a finite correlation extended above $T_N$ then $|A(\vec{q})|^2$ would have a finite value which might also be responsible for the enhancement of $1/(\chi T_1 T)$. If large enough single crystals could be grown, the origin of the enhancement could be conclusively resolved from inelastic neutron-scattering measurements of the magnetic fluctuation wave vector above $T_N$.

A sharp peak in $1/T_1$ versus $T$ is a direct indication of long-range magnetic ordering. However, the peak position for the $H=0.65$ T measurement is at 3.65 K while for 4.06 T it is enhanced to 3.93 K. We plotted these two points in the $H$ vs $T_N$ phase diagram reported in Ref. 24 obtained from heat-capacity measurements of $T_N(H)$ [see inset of Fig. 6(b)], where it is clearly seen that $T_N$ increases slightly with increasing $H$ from 0 to 7 T and then decreases with further increase in the field. This behavior is similar to that observed in FSL compound $BaCdVO(PO_4)_2$ (Ref. 25) as well as in nonfrustrated 2D antiferromagnet $Mn(HCOO)_2\cdot 2H_2O$ (see p. 388 of Ref. 47). Qualitatively, long-range magnetic ordering in low-dimensional and/or frustrated spin systems is suppressed by quantum fluctuations. Magnetic field suppresses these quantum fluctuations, therefore $T_N$ is slightly enhanced with increasing field. However, above 10 T the field is strong enough to partially suppress the antiferromagnetic ordering, hence $T_N$ is reduced. In the antiferromagnetic ordered state, $1/T_1$ is mainly driven by scattering of magnons off nuclear spins, leading to a power-law temperature dependence.[48,49] For $T \gg \Delta$, where $\Delta$ is the gap in the spin-wave spectrum in temperature units, $1/T_1$ either follows a $T^3$ behavior due to a two-magnon Raman process or a $T^5$ behavior due to a three-magnon process, while for $T \ll \Delta$, it follows an activated behavior $1/T_1 \propto T^2 \exp(-\Delta/T)$. As seen from Fig. 6(a), our $^{31}P1/T_1$ data in the lowest temperature region ($1.5 \leq T \leq 2.3$ K) follow a $T^3$ behavior rather than a $T^5$ behavior suggesting that the relaxation is mainly governed by the two-magnon Raman process. The lack of activated behavior down to 1.5 K indicates that the upper limit of $\Delta$ is 1.5 K. Therefore, the upper limit of the axial anisotropy $[D \approx \Delta^2/(|J_1|+|J_2|)]$ (Ref. 12) would be about 0.15 K.

The $^{31}P$ $1/T_1$ data and the hyperfine coupling constants determined above enable us to estimate the exchange couplings in the system under investigation. According to Moriya, the nuclear spin-lattice relaxation rate $1/T_1$ at sufficiently high temperature in a system with exchange-coupled local moments is constant and can be expressed within the Gaussian approximation of the correlation function of the electronic spin as[35,50]

$$\left(\frac{1}{T_1}\right)_{T\to\infty} = \frac{(\gamma_N g \mu_B)^2 \sqrt{2\pi} z' S(S+1)}{3\omega_E}\left[\frac{\left(\frac{A^a_{hf}}{z'}\right)^2 + \left(\frac{A^b_{hf}}{z'}\right)^2}{2}\right], \tag{7}$$

where $\omega_E=[\max(|J_1|,|J_2|)k_B/\hbar]\sqrt{2zS(S+1)/3}$ is the Heisenberg exchange frequency, $z$ is the number of nearest-neighbor spins of each $V^{4+}$ ion, and $z'$ is the number of nearest-neighbor $V^{4+}$ spins of the P1 site. In order to get the coupling of the P1 site to individual $V^{4+}$ spins, the total coupling is divided by $z'$. Since our measurements were done for $H \| c$, the hyperfine couplings in the $ab$ plane (i.e., $A^a_{hf}$ and $A^b_{hf}$) contribute to $1/T_1$. Therefore, we have taken the rms average of couplings along the $a$ and $b$ directions. The $z'$ in the numerator is due to the fact that the P1 site feels the fluctuations arising from all nearest-neighbor $V^{4+}$ spins. Using the relevant parameters ($A^a_{hf} \simeq 1882$ Oe/$\mu_B$, $A^b_{hf} \simeq 1251$ Oe/$\mu_B$, $z=4$, $z'=4$, $S=1/2$, and the high-temperature (25–100 K) relaxation rate of $(\frac{1}{T_1})_{T\to\infty} \simeq 127$ $s^{-1}$ for the P1 site) in Eq. (7), the magnitude of the maximum exchange coupling constant was calculated to be $\max(|J_1|,|J_2|) \simeq 8$ K. For a system with two different exchange mechanisms, the exchange frequency is mainly dominated by the larger exchange interaction. Therefore, in $Pb_2VO(PO_4)_2$, this value of $J$ should represent the dominant exchange constant $J_2$. Indeed, $\max(|J_1|,|J_2|) \simeq 8$ K is close to the value $J_2=(9.3\pm0.6)$ K obtained from the $K(T)$ analysis above.

TABLE II. Critical exponent $\beta$ expected for different universality classes. The value of $\beta$ listed for the 2D XY model is for a finite-size system.

| | $\beta$ | References |
|---|---|---|
| 3D Heisenberg | 0.367, 0.33, 35 | 47, 51, and 52 |
| 3D XY | 0.345, 0.31, 0.33 | 47, 51, and 53 |
| 3D Ising | 0.326, 0.325, 0.31 | 47, 51, and 53 |
| 2D XY | 0.231 | 54 |
| 2D Ising | 1/8 | 51 and 53 |

### C. Critical effects

The NMR spectrum measurements can give a precise estimate of the temperature dependence of sublattice magnetization, which cannot be obtained from static magnetization measurements. The temperature dependence of $H_{int}$ can potentially provide the critical exponent $\beta$ reflecting the universality class/spin dimensionality of the spin system. In $Pb_2VO(PO_4)_2$, due to partial filtering of AF fluctuations above $T_N$, our $1/T_1$ data restricted us from doing a detailed

analysis. The $\beta$ values expected for different spin and lattice dimensionalities are listed in Table II.[47,51–54] If we assume that the experimental $\beta$ value of $\approx$0.23 obtained above from the measurements on the single crystal is due to critical fluctuations, then the $\beta$ value is closer to the 2D XY than the three-dimensional (3D) models although the ordering is suggested to be a 3D order from the powder neutron diffraction measurements.[28] We suggest that our data are not sufficiently close to $T_N$ to reflect 3D critical behavior.[47] It is to be noted that the longitudinal $\mu$SR relaxation rate above $T_N$ in $Pb_2VO(PO_4)_2$ has been fitted well by this 2D XY model.[29] A tiny in-plane anisotropy can dominate the fluctuations if the dominant AF correlation length is large.[55] In the present case, $\chi(T)$ above $T_N$ is approximately isotropic, but it is possible that there might be a small anisotropy which is not visible in the experimental $\chi(T)$. In fact, strong in-plane correlation may also enhance 3D coupling along the $c$ direction.[56] Therefore to understand this issue, a precise estimation of in-plane spin anisotropy is required.

It is useful to compare our data with data for other layered compounds. A similar reduced value of $\beta$ close to the $\beta$ for the 2D Ising model has been observed before in several layered compounds, e.g., $K_2NiF_4$, $K_2MnF_4$, $K_2CoF_4$, $Rb_2MnF_4$, and $RbCoF_4$ (Ref. 47). In these compounds the weak Ising-type anisotropy is about two orders of magnitude larger than the interplanar coupling. Therefore it is argued that the long-range ordering is primarily induced by the strong anisotropy crossover from 2D Heisenberg to 2D Ising behavior, which precedes the 2D Ising to 3D Ising crossover that should occur close to $T_N$. Since the onset of such 3D ordering is still governed by the 2D processes, the phase boundaries that are observed should reflect the underlying 2D character. Whenever there is a 3D ordering, one must have 3D correlations sufficiently close to $T_N$. For instance, in $BaNi_2(PO_4)_2$, an exponent ($\beta$=0.33) close to 3D model was found near $T_N$ and another exponent ($\beta$=0.23) close to that of the 2D XY model was found a little bit away from $T_N$ (see p. 281 of Ref. 47). However, in some cases this 3D critical region is over such a narrow temperature range that it is not accessible experimentally. Such a scenario has been realized before in the frustrated antiferromagnetic square-lattice compound $Li_2VOSiO_4$. In this compound, neutron powder-diffraction experiments show that the ordering is 3D and the antiferromagnetic $ab$ layers are coupled ferromagnetically along the $c$ axis.[57] In contrast, a reduced value of $\beta$ close to the $\beta$ value of the 2D XY model has been reported from NMR measurements and the authors suggested that the transition to the columnar phase might be driven by the XY anisotropy.[12,13] Although our experimental observations below $T_N$ are similar to those reported for $Li_2VOSiO_4$, a proper explanation for this peculiar behavior is still lacking in all these vanadates. Therefore further experiments on high-quality single-crystalline materials are essential to address this issue.

## V. CONCLUSION

We performed $^{31}$P NMR measurements on $Pb_2VO(PO_4)_2$, which is a strongly frustrated 2D Heisenberg square-lattice compound. The exchange couplings were estimated reliably from $K(T)$ analysis to be $J_1=(-5.4\pm0.5)$ K and $J_2=(9.3\pm0.6)$ K. From the NMR spectral measurements, the ground state was detected to be columnar antiferromagnetic (CAF) type and is consistent with that expected from the phase diagram (Fig. 1) for $\alpha\equiv J_2/J_1\simeq-1.72$. The hyperfine coupling and $1/T_1$ above $T_N$ are consistent with the distortion of the $V^{4+}$ squares due to monoclinic crystal symmetry. We have measured the temperature dependence of the sublattice magnetization in the CAF ordered state from the line splitting. The critical exponent $\beta$ estimated from the sublattice magnetization was close to the value predicted for a 2D XY model. We did not observe any signature of magnetic/structural disorder in contrast to the neutron-scattering and $\mu$SR experiments on powder samples.[27–29] To gain more insight, further complementary experiments on single crystals are required. Due to the low-energy scale of the exchange interactions, this compound is also a potential candidate for high-field experiments, and for high-pressure experiments where one can tune the exchange couplings.

## ACKNOWLEDGMENTS

We thank P. Carretta, A. A. Tsirlin, and F. Becca for fruitful discussions and correspondence. Work at the Ames Laboratory was supported by the Department of Energy, Basic Energy Sciences, under Contact No. DE-AC02-07CH11358.

*Present address: School of Physics, Indian Institute of Science Education and Research, Thiruvananthapuram 695016, India.

[1] *Frustrated Spin Systems*, edited by H. T. Diep (World Scientific, Singapore, 2004).
[2] N. Shannon, B. Schmidt, K. Penc, and P. Thalmeier, Eur. Phys. J. B **38**, 599 (2004).
[3] N. Shannon, T. Momoi, and P. Sindzingre, Phys. Rev. Lett. **96**, 027213 (2006).
[4] B. Schmidt, N. Shannon, and P. Thalmeier, J. Phys.: Condens. Matter **19**, 145211 (2007).
[5] O. P. Sushkov, J. Oitmaa, and Z. Weihong, Phys. Rev. B **63**, 104420 (2001).
[6] S. Sorella, Phys. Rev. Lett. **80**, 4558 (1998).
[7] L. Capriotti and S. Sorella, Phys. Rev. Lett. **84**, 3173 (2000).
[8] L. Capriotti, F. Becca, A. Parola, and S. Sorella, Phys. Rev. Lett. **87**, 097201 (2001).
[9] Q. Si and E. Abrahams, Phys. Rev. Lett. **101**, 076401 (2008).
[10] X. H. Chen, T. Wu, G. Wu, R. H. Liu, H. Chen, and D. F. Fang, Nature (London) **453**, 761 (2008).
[11] Y. Kamihara, T. Watanabe, M. Hirano, and H. Hosono, J. Am. Chem. Soc. **130**, 3296 (2008).
[12] R. Melzi, S. Aldrovandi, F. Tedoldi, P. Carretta, P. Millet, and F. Mila, Phys. Rev. B **64**, 024409 (2001).
[13] R. Melzi, P. Carretta, A. Lascialfari, M. Mambrini, M. Troyer,

P. Millet, and F. Mila, Phys. Rev. Lett. **85**, 1318 (2000).
[14] H. Rosner, R. R. P. Singh, W. H. Zheng, J. Oitmaa, S.-L. Drechsler, and W. E. Pickett, Phys. Rev. Lett. **88**, 186405 (2002).
[15] H. Rosner, R. R. P. Singh, W. H. Zheng, J. Oitmaa, and W. E. Pickett, Phys. Rev. B **67**, 014416 (2003).
[16] H. Kageyama, T. Kitano, N. Oba, M. Nishi, S. Nagai, K. Hirota, L. Viciu, J. B. Wiley, J. Yasuda, Y. Baba, Y. Ajiro, and K. Yoshimura, J. Phys. Soc. Jpn. **74**, 1702 (2005).
[17] N. Oba, H. Kageyama, T. Kitano, J. Yasuda, Y. Baba, M. Nishi, K. Hirota, Y. Narumi, M. Hagiwara, K. Kindo, T. Saito, Y. Ajiro, and K. Yoshimura, J. Phys. Soc. Jpn. **75**, 113601 (2006).
[18] M. Yoshida, N. Ogata, M. Takigawa, J. Yamaura, M. Ichihara, T. Kitano, H. Kageyama, Y. Ajiro, and K. Yoshimura, J. Phys. Soc. Jpn. **76**, 104703 (2007).
[19] A. A. Tsirlin and H. Rosner, Phys. Rev. B **79**, 214416 (2009).
[20] P. Carretta, N. Papinutto, C. B. Azzoni, M. C. Mozzati, E. Pavarini, S. Gonthier, and P. Millet, Phys. Rev. B **66**, 094420 (2002).
[21] A. Bombardi, L. C. Chapon, I. Margiolaki, C. Mazzoli, S. Gonthier, F. Duc, and P. G. Radaelli, Phys. Rev. B **71**, 220406(R) (2005).
[22] A. A. Tsirlin, A. A. Belik, R. V. Shpanchenko, E. V. Antipov, E. Takayama-Muromachi, and H. Rosner, Phys. Rev. B **77**, 092402 (2008).
[23] E. E. Kaul, H. Rosner, N. Shannon, R. V. Shpanchenko, and C. Geibel, J. Magn. Magn. Mater. **272-276**, 922 (2004).
[24] E. E. Kaul, Ph.D. thesis, Technical University Dresden, 2005.
[25] R. Nath, A. A. Tsirlin, H. Rosner, and C. Geibel, Phys. Rev. B **78**, 064422 (2008).
[26] A. A. Tsirlin, B. Schmidt, Y. Skourski, R. Nath, C. Geibel, and H. Rosner, Phys. Rev. B **80**, 132407 (2009).
[27] M. Skoulatos, J. P. Goff, N. Shannon, E. E. Kaul, C. Geibel, A. P. Murani, M. Enderle, and A. R. Wildes, J. Magn. Magn. Mater. **310**, 1257 (2007).
[28] M. Skoulatos, J. P. Goff, C. Geibel, E. E. Kaul, R. Nath, N. Shannon, B. Schmidt, A. P. Murani, P. P. Deen, M. Enderle, and A. R. Wildes, EPL **88**, 57005 (2009).
[29] P. Carretta, M. Filibian, R. Nath, C. Geibel, and P. J. C. King, Phys. Rev. B **79**, 224432 (2009).
[30] R. V. Shpanchenko, E. E. Kaul, C. Geibel, and E. V. Antipov, Acta Crystallogr., Sect. C: Cryst. Struct. Commun. **62**, i88 (2006).
[31] A. A. Tsirlin and H. Rosner, Phys. Rev. B **79**, 214417 (2009).
[32] R. Nath, A. V. Mahajan, N. Büttgen, C. Kegler, A. Loidl, and J. Bobroff, Phys. Rev. B **71**, 174436 (2005); R. Nath, D. Kasinathan, H. Rosner, M. Baenitz, and C. Geibel, *ibid.* **77**, 134451 (2008); R. Nath, A. A. Tsirlin, E. E. Kaul, M. Baenitz, N. Büttgen, C. Geibel, and H. Rosner, *ibid.* **78**, 024418 (2008).
[33] Most people incorrectly write $K$ in terms of $\chi_{\mathrm{spin}}(\mathrm{cm}^3/\mathrm{mol})$ as $K(T)=K_0+\frac{A_{\mathrm{hf}}}{N_{\mathrm{A}}\mu_{\mathrm{B}}}\chi_{\mathrm{spin}}(T)$ with the units of $A_{\mathrm{hf}}$ expressed in $\mathrm{Oe}/\mu_{\mathrm{B}}$. In order to match units between the left- and right-hand sides of this expression, the units of $A_{\mathrm{hf}}$ should not be $\mathrm{Oe}/\mu_{\mathrm{B}}$, but rather Oe only. However, since Oe is the unit of hyperfine field and not of the hyperfine coupling constant, in order to have the correct units of $A_{\mathrm{hf}}(\mathrm{Oe}/\mu_{\mathrm{B}})$, the above expression should instead be written as $K(T)=K_0+\frac{A_{\mathrm{hf}}}{N_{\mathrm{A}}}\chi_{\mathrm{spin}}(T)$, with $\chi_{\mathrm{spin}}$ in units of $\mu_{\mathrm{B}}/(\mathrm{Oe\ mol})$.
[34] T. Förster (private communication).
[35] T. Moriya, Prog. Theor. Phys. **16**, 23 (1956).
[36] P. Carretta, T. Ciabattoni, A. Cuccoli, E. Mognaschi, A. Rigamonti, V. Tognetti, and P. Verrucchi, Phys. Rev. Lett. **84**, 366 (2000).
[37] P. Vonlanthen, K. B. Tanaka, A. Goto, W. G. Clark, P. Millet, J. Y. Henry, J. L. Gavilano, H. R. Ott, F. Mila, C. Berthier, M. Horvatic, Y. Tokunaga, P. Kuhns, A. P. Reyes, and W. G. Moulton, Phys. Rev. B **65**, 214413 (2002).
[38] F. Becca and F. Mila, Phys. Rev. Lett. **89**, 037204 (2002).
[39] C. Weber, F. Becca, and F. Mila, Phys. Rev. B **72**, 024449 (2005).
[40] Below 2.9 K, the satellites of the P1 site overlap with the satellites of the P2 site for both the $a$ and $b$ axes making the NMR lines indistinguishable.
[41] K. Kitagawa, N. Katayama, K. Ohgushi, M. Yoshida, and M. Takigawa, J. Phys. Soc. Jpn. **77**, 114709 (2008).
[42] K. Kitagawa, N. Katayama, K. Ohgushi, and M. Takigawa, J. Phys. Soc. Jpn. **78**, 063706 (2009).
[43] S.-H. Baek, N. J. Curro, T. Klimczuk, E. D. Bauer, F. Ronning, and J. D. Thompson, Phys. Rev. B **79**, 052504 (2009).
[44] T. Moriya, J. Phys. Soc. Jpn. **18**, 516 (1963).
[45] In Eq. (6), the hyperfine form factor corresponds to $\frac{A_{\mathrm{hf}}}{g\mu_{\mathrm{B}}}$ in Ref. 44.
[46] A. V. Mahajan, R. Sala, E. Lee, F. Borsa, S. Kondo, and D. C. Johnston, Phys. Rev. B **57**, 8890 (1998).
[47] *Magnetic Properties of Layered Transition Metal Compounds*, edited by L. J. de Jongh (Klewer, Dordrecht, 1989).
[48] D. Beeman and P. Pincus, Phys. Rev. **166**, 359 (1968).
[49] M. Belesi, F. Borsa, and A. K. Powell, Phys. Rev. B **74**, 184408 (2006).
[50] In several previous publications, the $(g\mu_{\mathrm{B}})^2=\gamma_e^2\hbar^2$ term in the numerator of Eq. (7) is left out which is present in the original equation in Ref. 35, where $\gamma_e$ the electronic gyromagnetic ratio. Absence of this term makes Eq. (7) dimensionally incorrect.
[51] M. F. Collins, *Magnetic Critical Scattering* (Oxford University Press, New York, 1989).
[52] A. Pelissetto and E. Vicari, Phys. Rep. **368**, 549 (2002).
[53] Y. Ozeki and N. Ito, J. Phys. A: Math. Theor. **40**, R149 (2007).
[54] S. T. Bramwell and P. C. W. Holdsworth, J. Phys.: Condens. Matter **5**, L53 (1993); Phys. Rev. B **49**, 8811 (1994).
[55] B. J. Suh, F. Borsa, L. L. Miller, M. Corti, D. C. Johnston, and D. R. Torgeson, Phys. Rev. Lett. **75**, 2212 (1995).
[56] H.-Q. Ding, Phys. Rev. Lett. **68**, 1927 (1992).
[57] A. Bombardi, J. Rodriguez-Carvajal, S. Di Matteo, F. de Bergevin, L. Paolasini, P. Carretta, P. Millet, and R. Caciuffo, Phys. Rev. Lett. **93**, 027202 (2004).